# Optimisation of a High Aspect-Ratio Transport Wing Using Coupled High-Fidelity Methods

Luís Miguel Martins Pacheco luis.miguel.martins.pacheco@tecnico.ulisboa.pt

Instituto Superior Técnico, Universidade de Lisboa, Portugal July 2025

#### Abstract

This work studies the influence of increasing the wing aspect ratio on the performance of modern transport aircraft and examines how different objective functions affect structural sizing design trade-offs. To this end, two high aspect-ratio composite medium-range transport aircraft wings underwent aeroelastic structural sizing, and their performances were compared. The optimisations were conducted using Airbus's in-house MDO suite and structural solver Lagrange and DLR's CFD solver TAU. Three objectives were considered: mass minimisation, aerodynamic efficiency maximisation, and Breguet range maximisation. A gradient-based algorithm with direct sensitivity analysis was used. Design variables, numbering approximately 3,000, included structural sizing parameters such as the thickness or cross-sectional area of the skin, spars, and stringers. Constraints reflected industry requirements, encompassing structural strength, buckling stability, and manufacturing criteria. Wing washout was induced solely with aeroelastic tailoring, promoting passive load alleviation through a bell-shaped lift distribution, effectively reducing the wing root bending moment. Manufacturing requirements constituted the most restrictive constraint in achieving further mass savings. For the investigated design points, the benefits of increasing the aspect ratio in modern transport aircraft were demonstrated, notably the improvement in aerodynamic efficiency and reduction in drag, despite the increase in structural weight. Furthermore, the markedly different design characteristics arising from different objective functions, and the value of a multidisciplinary performance-based objective in guiding early-stage design trade-offs were highlighted.

**Keywords:** multidisciplinary design optimisation, structural sizing, composite wings, aeroelastic tailoring.

# 1. Introduction

As global priorities shift towards ambitious climate objectives, sustainability becomes one of the aviation industry's foremost challenges. At the current pace, technological advancements fail to offset the rise in emissions caused by air traffic growth [1]. To address this issue, the development of novel environmentally sustainable aircraft is imperative.

High aspect-ratio wings (HARW) have emerged as a promising concept to improve aerodynamic efficiency. These designs reduce lift-induced drag, which accounts for about 40% of total drag in cruise for transport aircraft [2]. However, such configurations incur a structural weight penalty due to the higher wing root bending moment (WRBM) experienced in flight [3]. To effectively address this tightly coupled and conflicting set of design objectives, a multidisciplinary design optimisation (MDO) approach is necessary. In this work, these trade-offs are explored through a combined shape parameter study and structural sizing optimisation.

The goal is to investigate the influence of aspect ratio (AR) on the performance of modern transport aircraft and the impact of different objective functions on structural sizing trade-offs. To this end, two high aspect-ratio composite medium-range transport aircraft wings undergo structural sizing considering three objective functions: mass minimisation, aerodynamic efficiency maximisation, and Breguet range maximisation, and their performances are compared. This work uses Airbus's MDO suite and structural solver Lagrange [4] and DLR's CFD solver TAU [5].

# 2. Structural Sizing Framework for Minimum Mass

The approach used to solve the structural sizing involves two nested loops: an internal aeroelastic analysis loop and an external structural sizing optimisation loop.

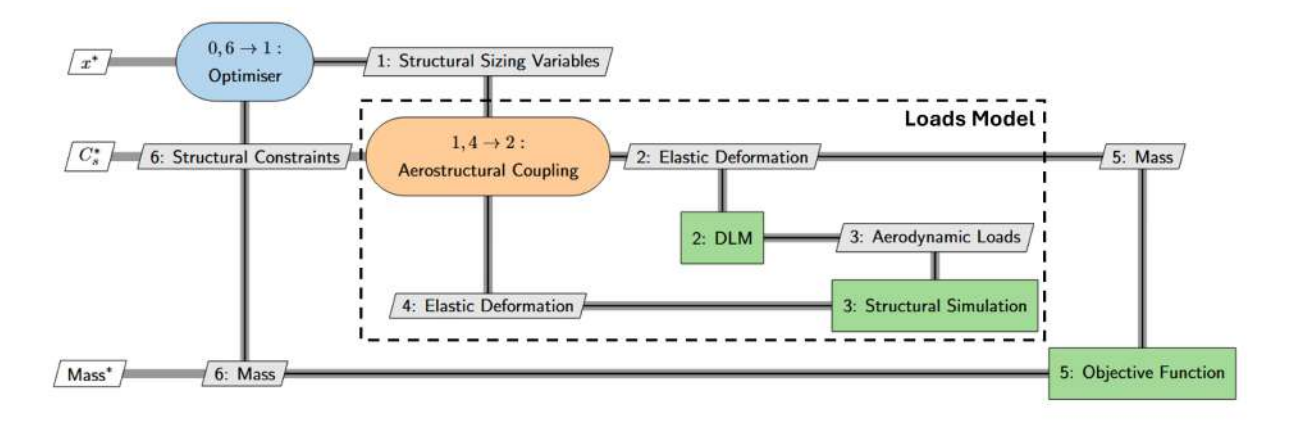


Figure 1: Structural sizing optimisation process for minimum mass.

## Aeroelastic Analysis

The structural sizing begins with an aerostructural analysis. The aerostructural coupling is handled in the form of a multidisciplinary analysis (MDA), posed as an iterative process that includes the fluid flow solution, load interpolation, structural deformation, and displacement transfer.

The process starts with the linear aerodynamic solution. The resulting loads are interpolated to the structural model. Using these aerodynamic forces, the structural problem is solved, yielding the elastic displacement field. These structural deformations are applied to the aerodynamic model, altering the lift distribution on the wing and starting over the iterative loop. After the coupling has converged, the structural constraints are evaluated.

#### Structural Sizing Optimisation

The structural constraint violations, and the structural mass, which can be directly obtained from the structural model without additional calculations, serve as input for the optimiser. The XDSM diagram for the structural sizing optimisation for minimum mass is illustrated in Figure 1.

## 2.1. Structural Model

The structural model must accurately represent the aircraft's stiffness and enable the assessment of structural sizing criteria. The response of the structure to applied loads is modelled using Hooke's law of linear elasticity

$$\boldsymbol{K} \cdot \boldsymbol{u} = \boldsymbol{f} \,, \tag{1}$$

where u represents the structure's displacement, f denotes the forces acting on the structural model, and K is its stiffness matrix. The structural problem is solved using the built-in finite element (FE) solver of Airbus's MDO suite Lagrange [4].

## 2.2. Aerodynamic Model

The doublet lattice method (DLM) [6] is used, as linear aerodynamic models offer sufficient accuracy

in lift load distribution estimates for structural sizing in the preliminary design stage at a low computational cost, without compromising the robustness of the optimisation process.

In the DLM, the doublet strengths  $\Gamma$  are determined by enforcing Neumann's boundary condition at the collocation point of each panel. The resulting system of equations is given by

$$AIC \cdot \Gamma = b_c, \qquad (2)$$

where AIC is the complex-valued aerodynamic influence coefficient matrix and  $b_c$  denotes the boundary conditions. After computing  $\Gamma$ , the lift force on each panel is calculated using the Kutta-Joukowski theorem.

The **AIC** matrix is generated from the DLM mesh and provided to Lagrange, which incorporates a linear aerodynamic analysis tool [4] capable of computing the aerodynamic loads.

# 2.3. Loads and Displacement Transfer

Due to distinct domain discretisation, the meshes at the fluid-structure interface typically do not match, preventing direct information exchange. To interpolate the structural displacements to the fluid flow mesh and the aerodynamic load information to the structural domain the infinite plate spline (IPS) method [7] is used.

# 2.4. Structural Sizing Criteria

A robust criteria model prevents optimisations from converging on impractical solutions. Adequately addressing the criteria model ensures a balance between structural weight and stiffness. The structural sizing criteria used encompasses:

- Strength requirements;
- Buckling requirements;
- Manufacturing requirements.

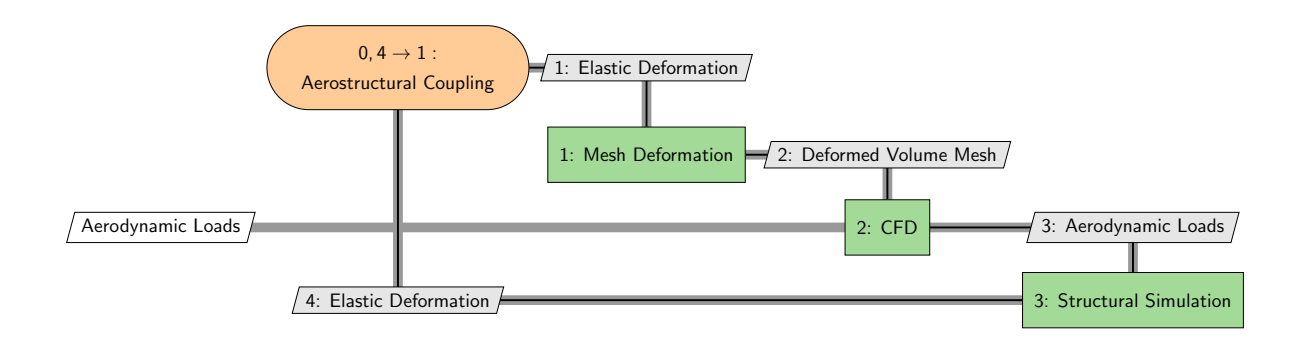


Figure 2: Coupled aerostructural analysis for performance evaluation.

The structural sizing criteria primarily focus on optimising the composite wing covers, as they are the main drivers of aeroelastic tailoring.

# 3. Aircraft Performance Analysis Framework

Following the completion of structural sizing for mass minimisation, the performance of both aircraft is analysed. To that end, a high-fidelity multidisciplinary design analysis and optimisation framework is used [8, 9]. This framework couples Airbus's MDO suite Lagrange [4] with DLR's CFD solver TAU [5] through the software integration platform FlowSimulator [10]. A description of the high-fidelity aerostructural analysis used for performance evaluation follows.

## 3.1. Aerostructural Analysis

The high-fidelity aerostructural analysis uses a three-field formulation of the coupled aerostructural problem, where mesh deformation is incorporated as an additional discipline alongside aerodynamic and structural analysis, as illustrated in Figure 2.

The aerostructural analysis begins with TAU solving the governing flow equations in a CFD simulation. The aerodynamic forces are then interpolated from the aerodynamic domain onto the structural mesh. Considering these aerodynamic forces, Lagrange's FE solver computes the structural deformations. These structural displacements are interpolated onto the aerodynamic surface mesh and applied as boundary conditions in the aerodynamic mesh deformation problem.

The convergence criterion of the coupling process is defined by the  $L^2$  norm of the variation in elastic deformation at the fluid-solid interface. The rate of convergence for the aerostructural coupling is improved through a dynamic under-relaxation using the standard Aitken  $\Delta^2$  method [11].

## 3.2. Structural Discipline

In the performance analysis, the structural problem is also governed by the equations of linear elasticity.

The structural residuum  $\mathcal{R}_S$  can be expressed as

$$\mathcal{R}_S = K y_S - f_S = 0, \qquad (3)$$

where K is the symmetric stiffness matrix,  $y_S$  is the state variables vector representing the structural displacement, and  $f_S$  is the sum of the forces acting on the structure.

The structural problem is solved using the builtin FE solver of Lagrange.

### 3.3. Aerodynamic Discipline

Several of the performance metrics to be analysed require drag. Since drag can only be reliably predicted using high-fidelity aerodynamics, a distinct aerostructural analysis from that used to drive the structural sizing is necessary.

In the high-fidelity analysis, the fluid problem is governed by the compressible Reynolds-averaged Navier-Stokes (RANS) equations, coupled with the Spalart-Allmaras (SA) one equation turbulence model in its negative formulation. The residuals of the governing flow equations are expressed as

$$\mathcal{R}_F = \frac{\partial y_F}{\partial t} + \nabla \cdot (\phi_c - \phi_v) = 0, \qquad (4)$$

where  $\phi_c$  and  $\phi_v$  are the convective and diffusive fluxes, respectively, and the state variables  $y_F$  denote the conserved quantities of the flow.

These equations are discretised with the finite volume method and solved using DLR's CFD solver TAU [5].

## 3.4. Loads and Displacement Transfer

A mesh-free approach based on the moving least squares (MLS) method [12] is used to interpolate the loads and displacements between the structural and aerodynamic domains. This method is both conservative and consistent.

### 3.5. Aerodynamic Mesh Deformation

The aerodynamic volume mesh must adapt to the deformation of its surface mesh induced by the structural displacement. The mesh deformation

method used is based on the linear elasticity analogy [13], whereby the fluid flow mesh is considered analogous to a volumetric structure problem.

The governing equation for mesh deformation is given by

$$\mathcal{R}_M = \mathbf{K}_M \mathbf{y}_M - \mathbf{f}_M(\mathbf{u}) = 0, \qquad (5)$$

where the state variables  $y_M$  denote the deformed mesh coordinates,  $K_M$  is a symmetric stiffness matrix constructed by assigning stiffnesses to each element of the fluid flow mesh, and  $f_M$  is a fictitious force imposing the Dirichlet boundary condition.

### 4. DLR-F25 Models

To investigate the impact of increasing the AR on aircraft performance, two aircraft models were structurally sized: the high AR DLR-F25 and its newly developed variant with an even greater AR.

#### 4.1. Baseline Geometric Model

The DLR-F25 is a single-aisle, narrow-body aircraft model with a high aspect-ratio wing, designed for the short-medium range market segment [14]. This model, seen in Figure 3, has been primarily developed by the DLR and it is based on the Airbus A321neo. The key characteristics of the baseline DLR-F25 wing are summarised in Table 1.



Figure 3: Outer geometry of the DLR-F25.

Its aspect ratio of 15.6 is significantly higher than that of conventional transport aircraft and its tip chord of 0.6 metres and small taper ratio of 0.12, result in a narrow wing compared to those of the Airbus A320 family.

The DLR-F25 has a carry-through wingbox extending through the fuselage. The wing comprises a two-spar design with 31 ribs per half-span and 11 stringers, which progressively taper as the wing narrows towards the tip. The ribs and stringers have a minimum pitch of 800 mm and 220 mm, respectively, to prevent buckling from becoming a dominant design constraint.

4.2. Higher Aspect-Ratio Variant Geometric Model The DLR-F25 baseline aircraft was modelled using a parametric geometry representation, wherein the position of structural components was defined relative to the wing's coordinate system. This enables the automatic adjustment of component positions in response to shape variations.

Leveraging that parametric geometry, a higher aspect-ratio variant of the DLR-F25 was generated by modifying the baseline wing shape using Airbus's in-house tool Descartes [15]. Descartes is a pre-processing tool capable of generating a parametric geometry model, from which it can derive the necessary input data for structural sizing, including structural and aerodynamic models, as well as the optimisation model itself.

In the higher aspect-ratio variant, the wing up to the kink section remained unaltered to preserve the wing-fuselage junction and the original pylon attachment configuration. Consequently, only the wing sections aft of the engine were modified. The new higher aspect-ratio DLR-F25 variant was generated in Descartes by stretching the baseline's outer wing segments, increasing the overall wingspan by 10%, as seen in Figure 4. This resulted in a 11.5% higher aspect ratio of 17.4 and a 7.5% larger wing area.

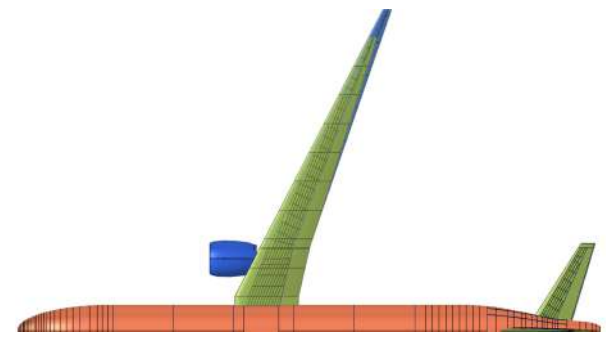


Figure 4: F25-AR17 shape change.

The leading-edge sweep and taper ratio were kept constant but the surface area increased. Maintaining the taper ratio was important, given that the DLR-F25's taper ratio was already small, and further reduction would pose aerodynamic challenges at the wingtip and could even obscure or counteract the impact of increasing the AR.

Henceforth, the baseline DLR-F25 and its higher aspect-ratio variant will be referred to as F25-AR15 and F25-AR17, respectively. Table 1 summarises the main geometrical differences between the model's wings.

The F25-AR17 aspect ratio increase altered the baseline rib pitch, resulting in significantly larger buckling fields. This rendered buckling a critical design constraint, precluding a fair direct compari-

Table 1: DLR-F25 wing key characteristics: baseline and higher aspect-ratio wings.

Parameter	Baseline	$\frac{\text{Higher AR}}{\text{F25-AR17}}$	
1 dramover	F25-AR15		
Aspect ratio	15.6	17.4	
Wingspan	$44.60 \mathrm{\ m}$	$49.04 \mathrm{m}$	
Wing area	$129.59 \text{ m}^2$	$139.21 \text{ m}^2$	
Sweep at $\frac{1}{4}$ chord	$24.43^{\circ}$	$24.69^{\circ}$	
Taper ratio	0.12	0.12	

son between the two aspect ratio variants. Consequently, a topological modification to the F25-AR17 wing was performed, wherein three additional ribs were incorporated, as illustrated in Figure 5.

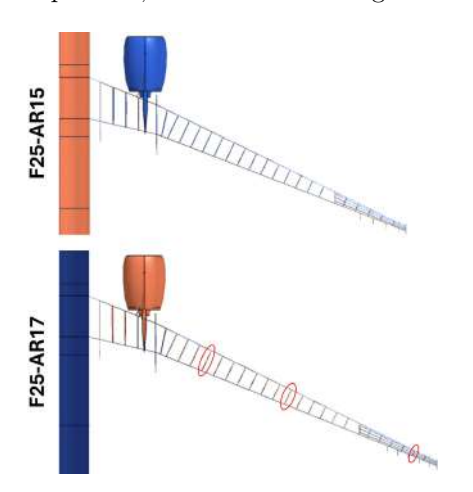


Figure 5: F25-AR17 topological change.

#### 4.3. Structural Models

The FE structural models were generated using Descartes' meshing functionality. As the structural problem for performance evaluation mirrors that of the structural sizing, the FE model used is the same.

The skins, spars, and ribs were modelled using CQUAD4 and CTRIA3 shell elements, whilst the stringers and spar caps were modelled using one-dimensional CBAR and CROD elements, respectively. The FE structural model for the F25-AR15 is depicted in Figure 6. The F25-AR17 model follows a comparable discretisation approach.

Two mass configurations are considered: the maximum take-off weight (MTOW) of 81,656 kg and the maximum zero fuel weight (MZFW) of 69,322 kg. The aircraft weight is divided into two components: the structural weight of the wing, determined by the size and material properties of its finite elements, and the weight of the fuel, payload, passengers, and the remaining aircraft structure, represented by concentrated mass points.

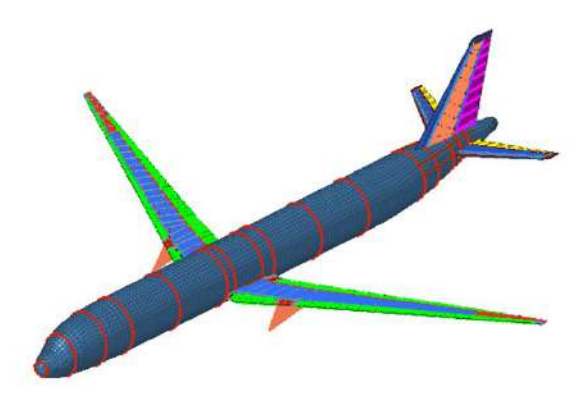


Figure 6: F25-AR15 FE structural model.

The wing skin is modelled using a symmetric and balanced 24-ply carbon fibre reinforced polymer (CFRP) laminate with four ply orientations (0°, 90°, and  $\pm 45^{\circ}$ ), and a density of 1,580 kg/m<sup>3</sup>. The T-shaped stringers and spar caps are modelled using homogenised CFRP properties, assuming a ply distribution of 70% at 0°, 20% at  $\pm 45^{\circ}$ , and 10% at 90°, with a density of 1,750 kg/m<sup>3</sup>.

## 4.4. Aerodynamic Models

Two levels of fidelity are used for the aerodynamic discipline: high-fidelity aerodynamics is used for performance analysis, whereas linear aerodynamics is used to drive the structural sizing optimisation.

In the DLM meshes the entire aircraft was discretised, as presented in Figure 7 for the F25-AR15. The wing was discretised into 7 panels in the chordwise direction and 43 panels in the spanwise direction. The discretisation for the F25-AR17 follows the same approach.

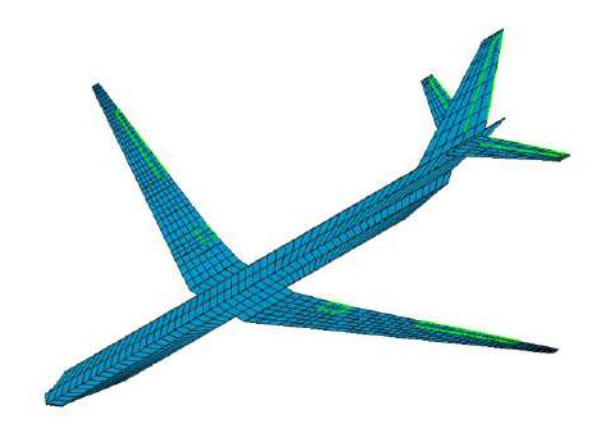


Figure 7: F25-AR15 doublet lattice method mesh.

The high-fidelity aerodynamic mesh is based on a wing-body configuration of the DLR-F25. A half-model of the aircraft is used to reduce the computational cost, leveraging the symmetry of the configuration, as illustrated in Figure 8 for the F25-AR15.

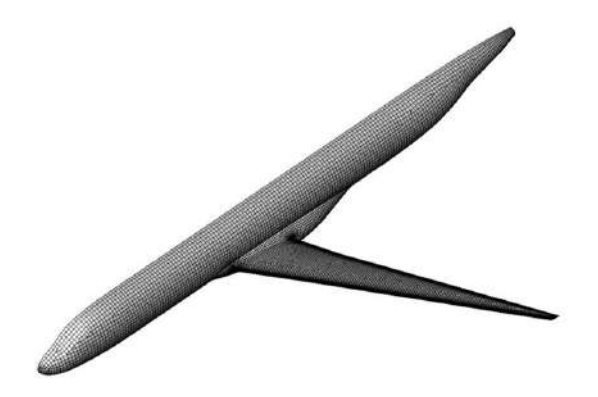


Figure 8: F25-AR15 high-fidelity aerodynamic surface mesh.

This computational grid, comprising 1.02 million nodes, was developed by the DLR. The mesh is quite coarse; however, it is suitable for the intended purpose. The aerodynamic model of the F25-AR17 was generated by morphing the F25-AR15 mesh.

#### 5. DLR-F25 Structural Sizing for Minimum Mass

The conventional structural sizing for wingbox structural mass minimisation was first performed.

### 5.1. Optimisation Problem

The optimisations are performed using the gradient-based NLPQL optimisation algorithm [16] with a coupled direct sensitivity analysis. The optimisations converge based on a Karush-Kuhn-Tucker (KKT) criterion of  $10^{-5}$ . An active-set strategy is implemented, restricting the sensitivity analysis to the 20,000 most violated constraints.

The optimisation focused exclusively on the structural sizing of the composite wingbox, specifically the wing skin, spars, and stringers.

The design variables are defined within patches. For the skin, each patch is bounded by two ribs and two stringers, whereas patches for the stringers and spars are segmented by ribs. These patches are symmetrically linked to ensure both sides of the wing are identical. Within each skin and spar web patch, plies of the same orientation are linked to preserve laminate symmetry. To ensure a balanced laminate, the thicknesses of the  $+45^{\circ}$  and  $-45^{\circ}$  plies are also linked. Consequently, three design variables per skin and spar web patch control the thickness of the ply orientations. The crosssectional area of each spar cap patch is governed by a single design variable. The T-shaped stringers are characterised by three design variables, which define the web height, foot width and thickness. The foot and web thickness are linked in a 1:2 ratio.

Constraints on strength, buckling, and manufacturability are incorporated into the structural sizing. Strength constraints are uniformly applied to

the skin, spars, and stringers, with maximum allowable material strains of  $5{,}000~\mu\varepsilon$  in tension and  $3{,}500~\mu\varepsilon$  in compression and a safety factor of 1.5 incorporated. The skin and spar buckling panels are modelled as biaxially loaded, simply supported flat plates with anisotropic material properties. The critical buckling loads are determined using analytical methods [17]. Stringer buckling is evaluated by modelling the stringer and attached sheet as a super-stiffener, with the critical buckling strength determined via the Johnson-Euler formula.

To ensure manufacturability, thickness and ply share constraints are imposed. Thickness variations between adjacent skin patches are limited by a ramp rate of 1:20 in the spanwise direction and 1:10 in the chordwise direction. Continuity constraints restrict thickness differences between adjacent plies to 1/10 of the ply thickness. Ply share percentages in the skin are constrained to a range of 10 to 63% for  $0^{\circ}$ and 90° plies and 20 to 80% for  $\pm 45^{\circ}$  plies. Additionally, a minimum thickness of 4 mm was enforced for the upper skin. On the lower skin, a minimum thickness of 20 mm was imposed in the pylon attachment area, with a 6 mm and 8 mm minimum thickness constraint outboard and inboard of this region. The size of the optimisation problems are summarised in Table 2.

Pull-up and push-over manoeuvres with the MTOW configuration were defined to be structurally design driving. These load cases were trimmed to balance pitching moment and ensure equilibrium between aerodynamic and inertial forces, with the angle of attack and elevator deflection serving as trimming variables. A summary of the load cases is presented in Table 3 [14].

# 5.2. Results

The primary focus of the structural sizing is the wing skin, as it plays a fundamental role in aeroelastic tailoring. Moreover, in this work, the wing skin is qualitatively representative of the changes on the stringers and spars.

Prior to structural sizing, both the F25-AR15 and F25-AR17 wings had generic uniform thicknesses. As expected, neither aircraft variant satisfied the imposed structural sizing criteria, with significant constraint violations observed near the wing root.

Having infeasible designs as a starting point, both aircraft variants underwent structural sizing for mass minimisation. In Table 4, the wingbox structural mass after structural sizing is presented.

The F25-AR17 wingbox is 5.51% (293 kg) heavier than the F25-AR15's due to the additional material required for its larger wing, as well as the increased thickness of its structural components at the wing root, necessary due to the 5.97% higher WRBM associated with the increased AR.

Table 2: Structural sizing optimisations problem size.

	Design Variables			Constraints				
	Skin	Spar	Stringer	Total	Strength	Buckling	Manufacturing	Total
F25-AR15	1,251	390	1,284	2,925	137,488	5,904	74,109	217,501
F25-AR17	1,353	470	$1,\!372$	$3,\!195$	$149,\!800$	$6,\!352$	81,025	$237,\!177$

Table 3: Load cases for structural sizing.

Load case	Load factor [g]	Mach	Altitude [m]
Pull-up Push-over	2.5 -1	0.81	11,000

Table 4: Wingbox structural mass after structural sizing.

	F25-AR15	F25-AR17
Wingbox Mass [kg]	5322	5615

The wing skin thickness of both aspect ratios is very similar, with the thickness increasing in the vicinity of the pylon region, where the loads are highest, and gradually tapering towards the wingtip. Different ply orientations are leveraged across various wing regions to manage loads effectively. The  $0^{\circ}$  and  $\pm 45^{\circ}$  plies form the majority of the laminate. The  $90^{\circ}$  plies play a less significant role, tending to the imposed minimum.

After structural sizing, no constraint violations were observed. Manufacturing requirements constitute the most dominant constraints, followed by strength and, subsequently, buckling criteria.

Overall, the structural sizing for mass yielded two feasible high aspect-ratio composite wings.

### 6. DLR-F25 Performance Analysis

The aerostructural analyses for performance were conducted under cruise conditions, at a Mach number of 0.78 and an altitude of 10,363 metres, corresponding to a Reynolds number of 22 million. The aircraft were trimmed to achieve a target lift force using a gradient-based approach with the angle of attack as design variable.

Wing washout was induced solely with aeroelastic tailoring, promoting passive load alleviation through a bell-shaped lift distribution, effectively reducing the WRBM. Figure 9 presents the twist distribution in cruise, suggesting that the washout is more pronounced as the AR increases.

This negative twist reduces the angle of incidence and, consequently, the lift generated at the wingtip, thereby shifting the loads inboard. This results in a bell-shaped lift distribution, illustrated in Figure 10, which shortens the aerodynamic lever arm.

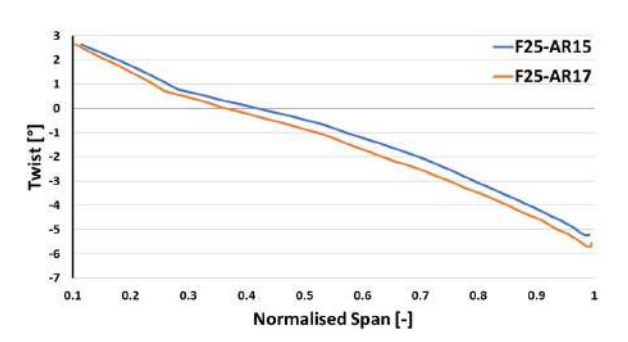


Figure 9: Twist distribution in cruise.

Consequently, the mass-driving maximum WRBM is reduced through passive load alleviation. This effect is more pronounced in the higher AR variant.

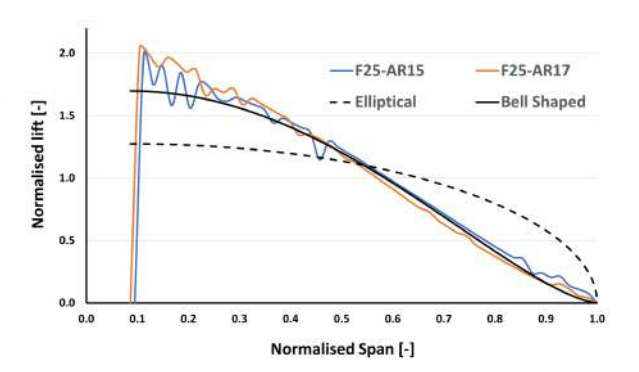


Figure 10: Lift distribution in cruise.

The F25-AR17 has a 2.18% higher aerodynamic efficiency highlighting the aerodynamic advantages of increasing the aspect ratio in the investigated design point. This can be attributed to the 2.14% reduction in drag associated with the higher AR.

The Breguet range of both aspect ratio aircraft was estimated. The F25-AR15 yielded a Breguet range of 4,666 km, while the F25-AR17 achieved a slightly longer Breguet range of 4,768 km.

## 7. DLR-F25 Structural Sizing for Maximum Aerodynamic Efficiency or Breguet Range

After completing the structural sizing for mass minimisation and evaluating the performance of both aspect ratios, two further objective functions are considered: the maximisation of aerodynamic efficiency, or the maximisation of Breguet range.

Aerodynamic efficiency is selected to provide a

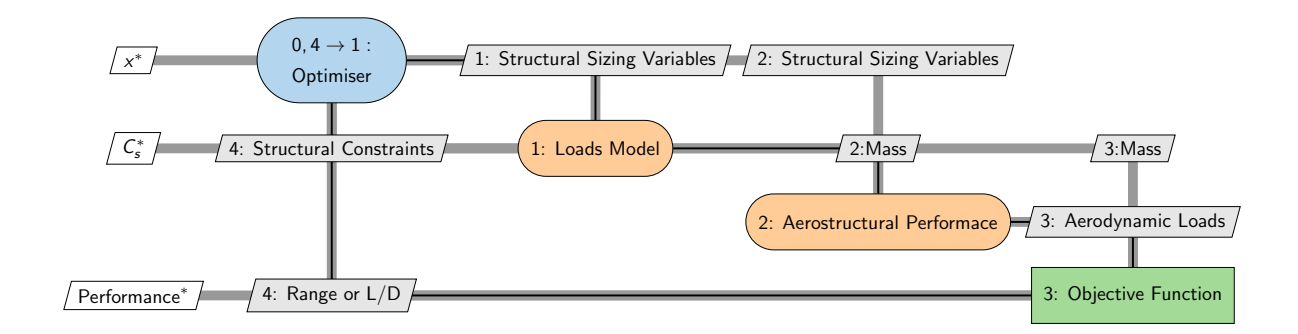


Figure 11: Structural sizing optimisation process for aerodynamic efficiency or Breguet range.

contrast with the conventional mass-minimisation approach and the Breguet range to provide a tradeoff between structural and aerodynamic metrics.

While the mass objective can be directly obtained from the structural model without additional calculations, the newly introduced objective functions require additional computations to estimate drag. Since drag can only be accurately predicted with high-fidelity aerodynamics, the new optimisations with drag-dependent objectives require a high-fidelity aerostructural analysis, such as the one used in the performance evaluation, to estimate the loads for the new objective functions.

Consequently, a new aerostructural design process is put in place, integrating the high-fidelity aerostructural analysis outlined in Section 3 within the structural sizing process described in Section 2. The XDSM diagram of the new optimisation process used for the aerodynamic efficiency or Breguet range objective is shown in Figure 11.

These new optimisation studies are conducted using the same high-fidelity MDO framework [8, 9] previously employed for the performance evaluation. The aerodynamic, structural, and coupling models used in both fidelity aerostructural analyses are consistent with those presented in Section 4. Furthermore, the problem definition remains identical to that outlined in Section 5.1, with the exception of the objective function.

The starting point for these new optimisations are the designs obtained from the structural sizing for mass, with the F25-AR15 results serving as the reference in the following optimisation studies.

7.1. Structural Sizing for Aerodynamic Efficiency The convergence history of the optimisations for aerodynamic efficiency is presented in Figure 12. The optimisations converged smoothly, however only the final iterations yielded feasible designs.

The aerodynamic efficiency of the F25-AR15 and F25-AR17 increases by 6.00% and 7.86%, respectively, albeit at the expense of a 1.89% and 3.54% heavier MTOW. This highlights the trade-off be-

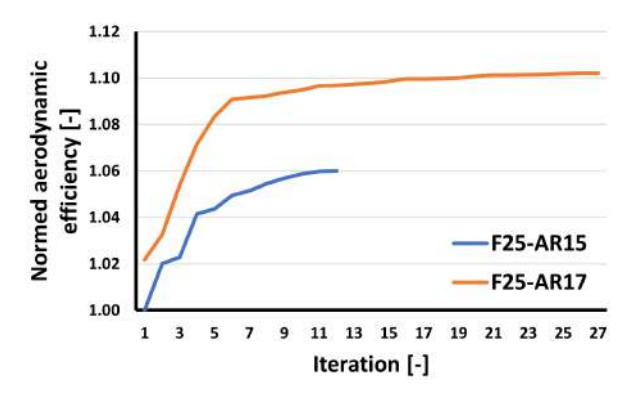


Figure 12: Convergence history of the structural sizing optimisations for aerodynamic efficiency.

tween aerodynamic gains and structural weight.

The improvements in aerodynamic efficiency are due to a reduction in pressure drag. This reduction arises from a more favourable lift distribution, with the centre of lift shifting outboard by more than 10%. However, this shift leads to an increase in WRBM and, thereby the mass.

The F25-AR17 has a 3.98% higher aerodynamic efficiency and a 3.83% lower drag than the F25-AR15, emphasising the advantages of increasing the aspect ratio at the investigated conditions.

# 7.2. Structural Sizing for Breguet Range

Figure 13 presents the convergence history of the structural sizing optimisations for Breguet range. The Breguet range improved by 4.73% and 5.23% for the F25-AR15 and F25-AR17, respectively. These optimisations achieve a lift-to-drag ratio similar to that obtained for the aerodynamic efficiency objective, whist providing a substantial MTOW reduction, highlighting the potential of the Breguet range to facilitate aerostructural trade-offs.

The F25-AR17 has a 3.38% higher aerodynamic efficiency and a 3.27% lower drag than the F25-AR15, highlighting again the aerodynamic advantages conferred by the higher AR in this context.

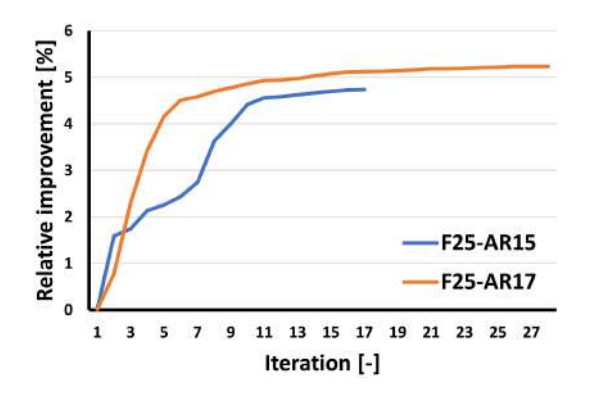


Figure 13: Convergence history of the structural sizing optimisations for Breguet range.

#### 7.3. Lift Distributions

Figure 14 illustrates the lift distributions after the structural sizing optimisations. All designs exhibit lift distributions that closely resemble the bell-shaped distribution. The structural sizing for mass shifts the loads inboard to reduce the WRBM, which is one of the main contributors to wing structural mass, through passive load alleviation. The other two optimisation cases produce lift distributions that start tending towards an elliptical profile, highlighting the prioritisation of drag reduction in these objectives.

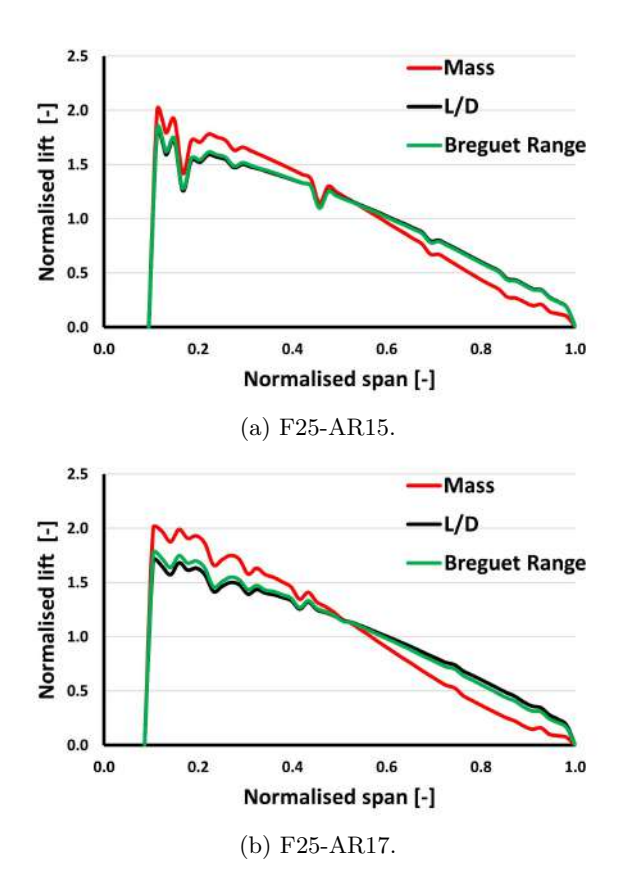


Figure 14: Lift distributions after structural sizing.

## 7.4. Pareto Fronts

Based on the three optimal designs corresponding to the distinct objective functions, Pareto fronts were estimated for each aspect ratio, as shown in Figure 15. Comparing the results of the optimisations focused on a single discipline objective, with those obtained by optimising for the Breguet range, the latter achieves a better trade-off between structural and aerodynamic efficiency in the investigated design points. Both aspect ratios offer markedly different characteristics in terms of mass and aerodynamic efficiency. For short-range missions, the F25-AR15 is more favourable due to its lower structural weight. Conversely, for longer missions, the F25-AR17 offers superior performance as a result of its improved aerodynamic efficiency.

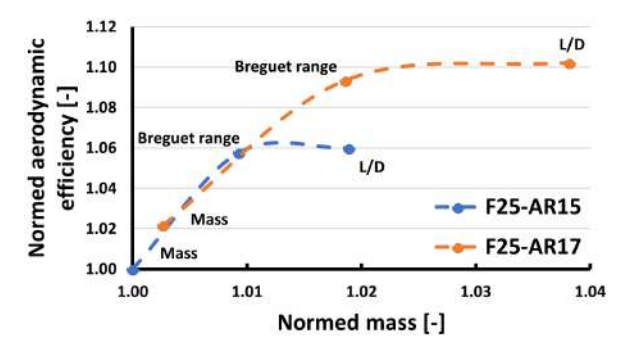


Figure 15: F25-AR15 and F25-AR17 Pareto fronts.

#### 8. Conclusions

The main objective of this work was to investigate the impact of increasing the aspect ratio on performance of modern transport aircraft. Additionally, the influence of different objective functions on structural sizing design trade-offs was assessed.

Wing washout was induced with aeroelastic tailoring, providing passive load alleviation through a bell-shaped lift distribution. This reduced the WRBM, a primary driver of structural mass in HARW. Manufacturing requirements were the most limiting criteria in achieving further mass savings.

For the investigated design points, the benefits of increasing the aspect ratio in modern transport aircraft were demonstrated, notably the improvement in aerodynamic efficiency and reduction in drag, despite the increase in structural weight. Furthermore, the results captured the markedly different design characteristics that arise from different objective functions, and the value of a multidisciplinary performance-based objective in guiding design trade-offs during the preliminary design stage.

Future work should expand the current shape parameter study to more aspect ratios, exploiting the opportunity to run these optimisations in parallel. Moreover, the design space should be widened to

include shape variables such as jig twist and aerofoil geometry. The integration of additional disciplines into the optimisation, particularly flight control, which is crucial for HARW, is strongly advised. A broader set of load cases, including gust encounters and aeroelastic phenomena like flutter, should be considered.

The main conclusion from this work is that MDO should serve to inform designers and support the decision-making process rather than to replace it. Achieving this requires critical interpretation of optimisation outcomes, treating the process not as a black box or panacea, but as a tool for gaining valuable insights into the design space.

#### References

- [1] Clean Aviation Joint Undertaking. Strategic Research and Innovation Agenda. Technical Report CAJU-GB-2021-12-16-SRIA, European Commission, December 2021.
- [2] I. Kroo. Drag due to lift: concepts for prediction and reduction. Annual review of fluid mechanics, 33:587-617, 01 2001. doi:10.1146/annurev.fluid.33.1.587.
- [3] G. K. W. Kenway and J. R. R. A Martins. Multipoint High-Fidelity Aerostructural Optimization of a Transport Aircraft Configuration. *Journal of Aircraft*, 51(1):144–160, 2014. doi:10.2514/1.C032150.
- [4] G. Schuhmacher, F. Daoud, Ö. Petersson and M. Wagner. Multidisciplinary Airframe Design Optimization. In 28th International Congress of the Aeronautical Sciences. Brisbane, Australia, September 2012.
- [5] D. Schwamborn, T. Gerhold, R. Heinrich. The DLR TAU-code: recent applications in research and industry. In ECCOMAS CFD Conference, Delft, Netherlands, 2006.
- [6] E. Albano and W. P. Rodden. A doublet-lattice method for calculating lift distributions on oscillating surfaces in subsonic flows. AIAA Journal, 7(2):279–285, 1969. doi:10.2514/3.5086.
- [7] R. L. Harder and R. N. Desmarais. Interpolation using surface splines. *Journal of Aircraft*, 9(2):189–191, 1972. doi:10.2514/3.44330.
- [8] F. Volle, M. Abu-Zurayk, A. U. Balani, S. Deinert and Ö. Petersson. Simultaneous Shape and Sizing Optimization for Improving Aircraft Performance Using the Aero-Structure Adjoint. In *Deutsche Luft- und* Raumfahrtkongress - DLRK, Stuttgart, Germany, September 2023.

- [9] A. A. Gastaldi, F. Volle, F. Daoud, C. Breitsamter. Simultaneous Airframe Shape and Sizing Optimization Using FlowSimulator and the Lagrange MDO Suite. In *Deutsche Luft- und* Raumfahrtkongress - DLRK, Dresden, Germany, September 2022.
- [10] M. Meinel and G. Ó. Einarsson. The FlowSimulator framework for massively parallel CFD applications. In Applied parallel and scientific computing 10th International Conference. Reykjavik, Iceland, June 2010.
- [11] U. Küttler and A. W. Wall. Fixed-point fluidstructure interaction solvers with dynamic relaxation. *Computational mechanics*, 43(1):61– 72, 2008. doi:10.1007/s00466-008-0255-5.
- [12] A. Schuster, L. Reimer and J. Neumann. A Mesh-Free Parallel Moving Least-Squaresbased Interpolation Method for the Application in Aeroelastic Simulations With the Flow Simulator. New Results in Numerical and Experimental Fluid Mechanics X, 132:573–583, 2016. doi:10.1007/978-3-319-27279-5\_50.
- [13] A. Rempke. Netzdeformation mit Elastizitätsanalogie in multidisziplinärer FlowSimulator-Umgebung. In Jahresbericht 2016 zum 20. DGLR-Fach-Symposium der STAB. Braunschweig, Germany, November 2016.
- [14] S. Wöhler, J. Häßy and V. Kriewall. Establishing the DLR-F25 as a research baseline aircraft for the short-medium range market in 2035. In 34th Congress of the International Council of the Aeronautical Sciences,. Florence, Italy, September 2024.
- [15] R. Maierl, Ö. Petersson, F. Daoud. Automated Creation of Aeroelastic Optimization Models from a Parameterized Geometry. In 15th International Forum on Aeroelasticity and Structural Dynamics, Bristol, UK, June 2013. Royal Aeronautical Society.
- [16] K. Schittkowski. NLPQL: A FORTRAN subroutine solving constrained nonlinear programming problems. Annals of operations research, 5:485–500, 1986. doi:10.1007/BF02022087.
- [17] P. M. Weaver. Approximate analysis for buckling of compression loaded long rectangular plates with flexural/twist anisotropy. Proceedings of the Royal Society A: Mathematical, Physical and Engineering Sciences, 462(2065): 59–73, 2006. doi:10.1098/rspa.2005.1552.